

LASER BIOLOGY AND MEDICINE

PACS numbers: 42.30.Wb; 42.25.Dd; 87.57.Gg; 87.63.Lk
DOI: 10.1070/QE2002v032n11ABEH002325

Visualisation of details of a complicated inner structure of model objects by the method of diffusion optical tomography

E.V. Tret'yakov, V.V. Shuvalov, I.V. Shutov

***Abstract*. An approximate algorithm is tested for solving the problem of diffusion optical tomography in experiments on the visualisation of details of the inner structure of strongly scattering model objects containing scattering and semitransparent inclusions, as well as absorbing inclusions located inside other optical inhomogeneities. The stability of the algorithm to errors is demonstrated, which allows its use for a rapid (2 – 3 min) image reconstruction of the details of objects with a complicated inner structure.**

Keywords: *optical tomography, light propagation in a scattering medium, image visualisation.*

1. Diffusion optical tomography

In optical tomography (OT), which is a new trend in diagnostics rapidly developing in the last years, an object is illuminated many times (at different positions of a radiation source i and a detector j) by near-IR radiation. The parameters of transmitted radiation (the radiation power, the pulse energy and shape, the pulse delay with respect to the instant of its incidence on the object, etc.) are measured for all combinations of i and j. As a result, the matrix $\{\Phi_{i,j}\}$ of the output data is obtained. The number of matrix elements is determined by the number of positions of the radiation source and detector. This matrix is used for the reconstruction of the inner structure of the object, i.e., the so-called inverse problem is solved. The absorption (μ_a) and scattering (μ'_s) coefficients, the anisotropy parameter γ of the scattering indicatrix and some other quantities play the role of physical parameters whose spatial distributions are being reconstructed at this stage.

Even in the case of multiple small-angle scattering [1, 2], a contribution of photons propagating from the point i to the point j (hereafter, the i, j measurement) almost along linear trajectories can be separated from a total output radiation flux [3, 4]. In this case, the inverse problem can be solved by using algorithms that were developed for projection X-ray tomography [5, 6]. Most OT methods (for example, time-of-flight [7 – 9], coherent [10 – 12], and frequency-domain [13 – 15] OT) differ in the ways of such separation. A peculiarity of diffusion OT (DOT) is that it uses the total output radiation flux. As a result, the diagnostics of much larger objects can be performed, other conditions being the same, which is a main advantage of this method. However, there also exists a serious problem. Photons detected in the i, j measurements are propagating along random trajectories, and therefore should be described statistically with the help of the 3D probability distributions $f_{i,j}(\boldsymbol{r})$ for the propagation of photons through different (coordinate $\boldsymbol{r}$) points in the object. However, because the width of these distributions is finite, DOT allows the reconstruction of the inner structure of an object [16 – 21].

E.V. Tret'yakov, V.V. Shuvalov, I.V. Shutov International Teaching and Research Laser Center, M.V. Lomonosov Moscow State University, Vorob'evy gory, 119992 Moscow, Russia

Received 11 July 2002
Kvantovaya Elektronika **32** (11) 941 – 944 (2002)
Translated by M.N. Sapozhnikov

2. Approximate algorithm for solving the DOT problem

A fast approximate algorithm for solving the DOT problem described in papers [22 – 24] assumes that $\Delta\Phi_{i,j}^{(1)} = \Phi_{i,j}^{(1)} - \Phi_{i,j}$, the difference of output radiation fluxes (hereafter, 'shadow') in the absence of opaque inhomogeneities (inclusions, $\Phi_{i,j}^{(1)}$) and in the presence of them ($\Phi_{i,j}$), is caused by the appearance of inhomogeneities. It is assumed that the probability of finding inclusions from each i, j measurement is $P_{i,j}^{(1)} \propto \Delta\Phi_{i,j}^{(1)}$, and the spatial distribution of $P_{i,j}^{(1)}$ is defined as $p_{i,j}^{(1)}(\boldsymbol{r}) \propto P_{i,j}^{(1)} f_{i,j}^{(1)}(\boldsymbol{r})$, where $f_{i,j}^{(1)}(\boldsymbol{r})$ is the distribution of the probability of passing of photons detected in the i, j measurement through the object without inclusions ($\mu_a, \mu'_s = \text{const}$).

The reconstructed inner structure is described by the distribution $p_{\Sigma}^{(1)}(\boldsymbol{r})$ of the probability of finding inclusions at different points of the object, which is proportional to $\prod_{i,j} P_{i,j}^{(1)} f_{i,j}^{(1)}(\boldsymbol{r})$ according to the results of all the i, j measurements. A priory information on the functions $f_{i,j}^{(1)}(\boldsymbol{r})$ and $\Phi_{i,j}^{(1)}$ required for the algorithm is calculated approximately. For this purpose, the only calculated 'standard' distribution $f_L^{(1)}(\boldsymbol{r})$ for an object without inclusions is approximated by a smooth function of $\boldsymbol{r}$ with the Gaussian cross sections, which is successively transformed [scaled, 'bent', and normalised; $f_L^{(1)}(\boldsymbol{r}) \to f_{L_{i,j}}^{(1)}(\boldsymbol{r}) \to f_{i,j}^{(1)}(\boldsymbol{r})$, taking into account a change in the distance between a radiation source and a detector ($L \to L_{i,j}$) and their specific positions i and j]. Upon bending, the generating (axial) lines of the distributions $f_{i,j}^{(1)}(\boldsymbol{r})$ are described by parabolas, and the calculation time of a complete data array of 1024 ($0 \leqslant i, j \leqslant 31$) such distributions is less than 30 s. The elements of the matrix $\{\Phi_{i,j}^{(1)}\}$ also are calculated approximately using empirical properties described in paper [22].

The testing of this algorithm showed [23] that, in the presence of several opaque inclusions of different sizes in an object, only the largest details of the structure could be reconstructed. This problem can be solved by using the second iteration in the algorithm, in which a priory information is calculated taking into account the details of the inner structure reconstructed during the first iteration [23, 24]. It is assumed that $\Delta\Phi_{i,j}^{(2)} = \Phi_{i,j}^{(2)} - \Phi_{i,j}$ – the difference of the radiation fluxes in the presence of reconstructed details, information on them being contained in $p_{\Sigma}^{(1)}(\boldsymbol{r})$, and the fluxes obtained experimentally is caused by the reconstruction errors, and the total probability of finding the error in the i, j measurement is $P_{i,j}^{(2)} \propto \Delta\Phi_{i,j}^{(2)}$. It is also assumed that the spatial distribution of $P_{i,j}^{(2)}$ is determined by the 3D probability density $p_{i,j}^{(2)}(\boldsymbol{r}) \propto P_{i,j}^{(2)} f_{i,j}^{(2)}(\boldsymbol{r})$, where $f_{i,j}^{(2)}(\boldsymbol{r})$ is the distribution of the probability of passing of photons, detected in the i, j measurement, through an object with a structure defined by the function $p_{\Sigma}^{(1)}(\boldsymbol{r})$. The inner-structure details reconstructed after the second iteration are described by the probability density $p_{\Sigma}^{(2)}(\boldsymbol{r})$, which is defined as $p_{\Sigma}^{(2)}(\boldsymbol{r}) \propto \prod_{i,j} P_{i,j}^{(2)} f_{i,j}^{(2)}(\boldsymbol{r})$ according to the results of all the i, j measurements.

The required *a priori* information on the functions $f_{i,j}^{(2)}(\boldsymbol{r})$ and $\Phi_{i,j}^{(2)}$ is also calculated approximately by using the above-described successive transformations of the 'standard' distribution $f_{\mathrm{L}}^{(1)}(\boldsymbol{r})$ and 'cutting out' (which is possible due to a linearity of the propagation problem) the absorbed part $p_{\Sigma}^{(1)}(\boldsymbol{r})$ of the photon flux $\Phi_{i,j}^{(1)}$ by inclusions reconstructed after the first iteration [23, 24]. The resulting inner structure is described by the superposition $p_{\Sigma}(\boldsymbol{r}) = p_{\Sigma}^{(1)}(\boldsymbol{r}) + p_{\Sigma}^{(2)}(\boldsymbol{r})$, which can be calculated in the case of two absorbing inclusions by using the total data array of 1024 ($0 \leqslant i, j \leqslant 31$) distributions $f_{\Sigma}^{(2)}(\boldsymbol{r})$ and fluxes $\Phi_{i,j}^{(2)}$ for less than 2 min. If necessary, next iterations can be used in the algorithm described.

3. Formulation of the problem

The applicability of the above-described procedure for the reconstruction of the inner structure of strongly scattering objects by the DOT method in several simplest experimental situations with opaque inclusions was demonstrated in papers [22–24]. Below, we describe the application of this algorithm in experiments on the visualisation of the inner structure of strongly scattering objects with more complicated inclusions (strongly scattering and semitransparent inclusions, and systems in which a part of inclusions is either indiscernible by the DOT method or located inside other semitransparent optical inhomogeneities). We will show that, after some corrections, the algorithm provides the reconstruction by the DOT method of the inner structure of strongly scattering objects containing absorbing and scattering inclusions.

4. Experimental

Radiation from a 30-mW, 820-nm cw diode laser was delivered through one of the 31 fibres of an optical 'switch' to an object under study, which represented a black cylindrical vessel of diameter 140 mm and height 170 mm. Optical fibres (31 input fibres and one output fibre) were glued to the side walls of the vessel at its half-height. A two-component (aqueous fat emulsion and ink) strongly scattering and weakly absorbing liquid ($\mu_{\mathrm{s}}' \simeq 1.4\ \mathrm{mm}^{-1}$ and $\mu_{\mathrm{a}} = 0.005\ \mathrm{mm}^{-1}$) was poured into the vessel and inclusions were added. The inclusions were black opaque cylinders of diameter 9 mm, a Teflon rod of diameter 8 mm, and chicken bones of diameters 8 and 10 mm. In addition, we could place into the vessel a ball of thin metal wire (the wire diameter was smaller than the spatial resolution) of diameter 110 mm, which simulated a capillary system, or a thin-wall (the wall thickness was 1 mm) hollow strongly scattering plastic cylinder of diameter 81 mm, which simulated a scull. The output radiation was delivered through a fibre to a Hamamatsu R-636-10 photomultiplier operating in the photon counting mode. Because the position of the output fibre was fixed, the positions of inclusions were changed appropriately during the object scanning. For this purpose, the inclusions were mounted on a movable cover of the vessel, which was rotated around its axis during scanning. The experimental data were accumulated, controlled, and processed with a PC. As a result of measurements, we obtained the 31×32 matrix $\{\Phi_{i,j}\}$ of the input data.

5. Experimental results

All the measurements were performed using the same procedure. First we measured the dependence of the photocounting rate $\Phi_{i,j_0}^{(1)}$ on the position of the point of radiation coupling ($1 \leqslant i \leqslant 31$) in the vessel with a strongly scattering and weakly absorbing liquid in the absence of inclusions for an arbitrary position of the cover ($j = j_0$). Taking into account the axial symmetry of the object, all the other elements of the matrix $\{\Phi_{i,j}^{(1)}\}$ ($1 \leqslant j \leqslant 32$) were found by the cyclical permutation of the elements of a column $\Phi_{i,j_0}^{(1)}$. Then, a complete scan ($1 \leqslant i \leqslant 31$, $1 \leqslant j \leqslant 32$) of the object with inclusions was performed, and the matrix $\{\Phi_{i,j}\}$ was found. The elements of the matrix $\{\Delta\Phi_{i,j}^{(1)}\}$ were calculated from these two measurements and then were used as the input data in the visualisation algorithm described above.

When the inclusions had a complicated structure, the second measurement was divided into two–three stages. Along with the measurements of the matrix elements $\{\Phi_{i,j}\}$ for the object with a 'complete' set of inclusions, the distributions of photocounting rates were also determined for 'incomplete' sets. For example, when two opaque inclusions were placed inside the scattering plastic cylinder in the object, the measurements were performed both for the object with two inclusions without the cylinder and for the object with the cylinder but without inclusions. The results of these measurements were used in the second iteration or for testing the applicability of the above-described algorithm for a fast approximate calculation of the matrix $\{\Phi_{i,j}^{(2)}\}$ in the presence of semitransparent or scattering inclusions, or directly as *a priori* information on the matrix $\{\Phi_{i,j}^{(2)}\}$.

As mentioned above, upon a fast approximate solution of the DOT problem (calculation of $\Phi_{i,j}^{(2)}$) for objects containing opaque inclusions, a part of the photon flux $\Phi_{i,j}^{(1)}$ propagating through points in the object occupied by inclusions is completely 'cut out' from the corresponding cross sections of the distributions $f_{i,j}^{(1)}(\boldsymbol{r})$. In the case of semitransparent inclusions (absorbing a part of propagating photons) this part of the photon flux can be partially 'cut out' from $f_{i,j}^{(1)}(\boldsymbol{r})$ due to the linearity of the propagation problem, by introducing an additional weight factor – the

transmission coefficient of an inclusion. Fig. 1 shows the first- and second-iteration reconstructions of the inner structure of an object with two inclusions – chicken bones of diameters 10 and 8 mm, which were obtained with the help of the modified algorithm described above. The geometrical positions and sizes of the reconstructed images of the inclusions very accurately correspond to the real geometry of the object.

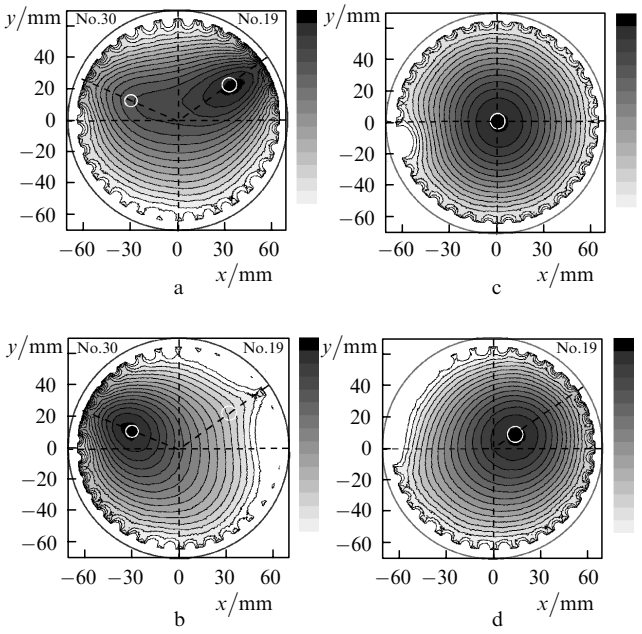

Figure 1. Visualisation of two semitransparent inclusions (chicken bones of diameters 10 and 8 mm) after the first (a) and second (b) iterations, and the visualisation of a scattering inclusion (Teflon rod of diameter 8 mm) for two experimental geometries (c, d). Here and in other figures, white circles are the real positions of inclusions and the number of the figure corresponds to the fibre number on the model object.

The inner structure of objects containing strongly scattering inclusions can be reconstructed in the same way. The matter is that the photocounting rate in the 'shadow' region (a photodetector is placed behind a scattering inclusion) will be also lower in this case than for an object without inclusions. However, because now the inclusion only scatters photons without absorbing, a part of these 'lacking' photons will be still detected, although beyond the 'shadow' region. This means that, unlike the case of an object with a partially absorbing inclusion considered above, the photocounting rate for other (side) positions of the detector should increase. In the case of strong scattering (to a large solid angle), an increase in the flux of photons detected in side detector positions will be rather small to be neglected in the following data processing. Therefore, although the geometrical position and size of the image of a strongly scattering inclusion (a Teflon rod of diameter 8 mm) (Figs 1c, d) reconstructed with the help of the above-described algorithm almost exactly coincide with the geometry of the real object, the image itself is reconstructed so that as if the inclusion is partially absorbing.

Experiments with a more complicated system of inclusions proved the versatility and stability of the approximate algorithm described above. Figs 2 and 3 illustrate the arrangement of two opaque inclusions of diameter 9 mm in an object and the result of the successive reconstruction (the first and second iterations) of the inner structure of the object in the absence (Fig. 2) and in the presence (Fig. 3) of a capillary system (a ball of thin wire) indiscernible in DOT. One can see that the position and size of the inclusion are reconstructed after the first iteration with errors (Figs 2b and 3b). Therefore, the size and position of this inclusion were slightly changed during the second iteration: the diameter and the distance from the axis were 9 and 30 mm, respectively (Figs 2c, 3c) and 12 and 20 mm,

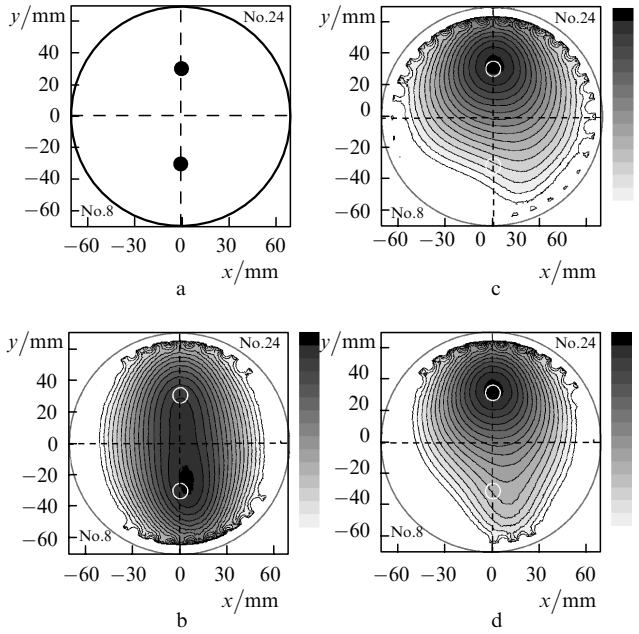

Figure 2. Geometry of the experiment (a) and visualisation of two opaque inclusions of diameter 9 mm after the first (b) and second (c, d) iterations taking into account the results of the first iteration.

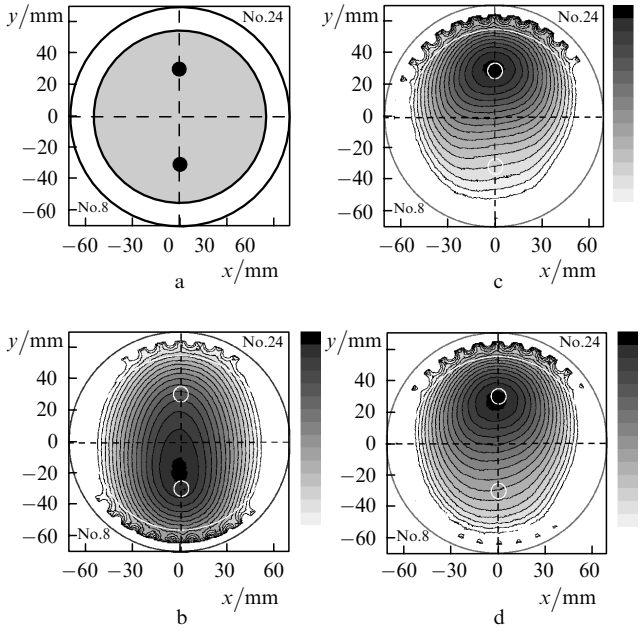

Figure 3. Geometry of the experiment (a) and visualisation of two opaque inclusions of diameter 9 mm in the model with a capillary system after the first (b) and second (c, d) iterations for two positions and sizes of the inclusion reconstructed after the first iteration.

respectively (Figs 2d, 3d). The experiment showed that the reconstruction algorithm is weakly sensitive to errors introduced at the first iteration, and the image of the second inclusion is reconstructed almost exactly after the second iteration. One can easily see that an absorbing capillary system indiscernible in DOT and placed inside the object (Fig. 3) does not prevent the accurate reconstruction of images of opaque inclusions.

As in the experiment with a Teflon rod described above, the image of a strongly scattering hollow cylinder of diameter 81 mm was reconstructed by the algorithm as a weakly absorbing inclusion of the corresponding size (Fig. 4a). Moreover, the inner structure of a model object with a scattering cylinder and an opaque inclusion of diameter 9 mm was accurately reconstructed already after the first iteration (Fig. 4b). In this case, the second iteration of the algorithm, which takes into account cutting out a part of the detected photon flux by a semitransparent (the transmission coefficient 0.8) inclusion of diameter 81 mm (Fig. 4c) or uses the input matrix $\{\Delta\Phi_{i,j}^{(2)}\}$ representing the difference of two real matrices obtained in experiments in the absence of a strongly absorbing inclusion and in its presence, accurately reconstructs the object image.

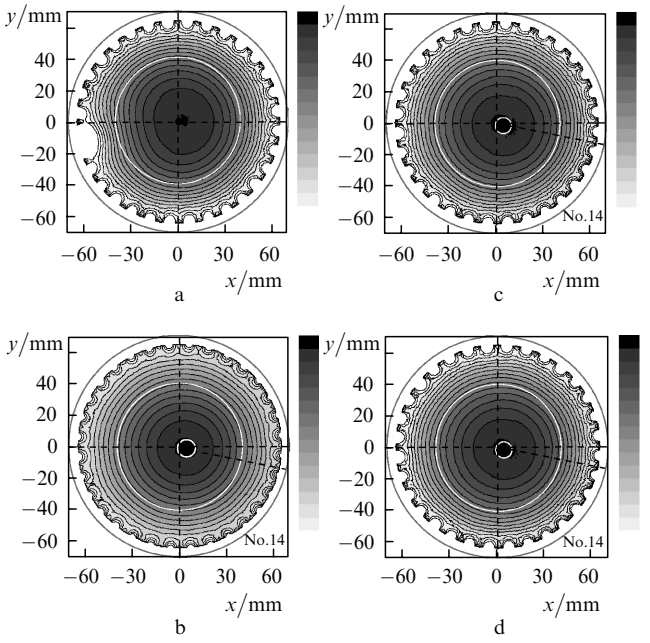

Figure 4. Visualisation of a hollow scattering cylinder of diameter 81 mm after the first iteration in the absence (a) and presence (b) of an opaque inclusion of diameter 9 m; the same for the input matrix (c) representing the difference of matrices for cases (a) and (b), as well as the second iteration (d) with 'cutting out' of photons by a semitransparent inclusion of diameter 81 mm with the transmission coefficient 0.8.

6. Conclusions

We have tested a fast approximate algorithm for the DOT reconstruction of the inner structure of strongly scattering model objects with inclusions of different types (strongly scattering and semitransparent inclusions, and inclusions that are either indiscernible in DOT or are located inside other optical inhomogeneities) and have shown that this algorithm, modified in an appropriate way, is not only stable to errors but also allows the reconstruction of the inner structure of objects with semitransparent and strongly scattering inclusions. The errors appearing at the first iteration of the algorithm due to its nonlinearity can be evidently corrected with the help of a similar third iteration performed taking into account the inner structure described by the function $p_{\Sigma}^{(2)}(\boldsymbol{r})$ reconstructed after the second iteration. These procedures are performed in a short time. It is important from the practical point of view that we used in all experiments low-cost, cw, low-power (up to 30 mW) diode lasers emitting in the near-IR region.

Acknowledgements. This work was supported by the Russian Foundation for Basic Research (Grant Nos 00-15-96726 and 01-02-17305).

References

1. Chance B. (Ed.) *Photon Migration in Tissues* (New York: Plenum Press, 1989).
2. Tuchin V.V. *Usp. Fiz. Nauk*, **167**, 541 (1997).
3. Ho P.P., et al. *Opt. and Photon. News*, **4**, 23 (1993).
4. Feng S.C., et al. *Proc. SPIE Int. Soc. Opt. Eng.*, **1888**, 78 (1993).
5. Herman G.T. *Image Reconstruction from Projections: the Fundamentals of Computerized Tomography* (San Francisco: Academic Press, 1980).
6. Sabatier P.C. *Basic Methods of Tomography and Inverse Problems: a Set of Lectures* (Bristol: Hilger, 1987).
7. Wang L., et al. *Science*, **253**, 769 (1991).
8. Proskurin S.G., et al. *Proc. SPIE Int. Soc. Opt. Eng.*, **2389**, 157 (1995).
9. Wells K., et al. *Proc. SPIE Int. Soc. Opt. Eng.*, **2979**, 599 (1997).
10. Tearney G.J., et al. *Proc. SPIE Int. Soc. Opt. Eng.*, **2389**, 29 (1995).
11. *Proc. SPIE Int. Soc. Opt. Eng.*, **2732** (1996).
12. *Proc. SPIE Int. Soc. Opt. Eng.*, **3915** (2000).
13. Sevick-Muraca E.M., et al. *SPIE Institutes for Advanced Optical Technologies* (Bellingham, 1993) Vol. 11, p. 485.
14. O'Leary M.A., et al. *Opt. Lett.*, **20**, 426 (1995).
15. Papaioannou D.G. *Proc. SPIE Int. Soc. Opt. Eng.*, **2626**, 218 (1995).
16. Lyubimov V.V., et al. *Proc. SPIE Int. Soc. Opt. Eng.*, **3566**, 57 (1998).
17. Lyubimov V.V., et al. *Proc. SPIE Int. Soc. Opt. Eng.*, **3816**, 183 (1999).
18. Gryazin Y.A., et al. *Inverse Problems*, **15**, 373 (1999).
19. Jong C., et al. *J. Opt. Soc. Am. A*, **16**, 2400 (1999).
20. Millane R.P., et al. *Proc. SPIE Int. Soc. Opt. Eng.*, **34123**, 295 (2000).
21. Markel V.A., Schotland J.C. *J. Opt. Soc. Am. A*, **18**, 1336 (2001).
22. Shuvalov V.V., et al. *Laser Phys.*, **11**, 636 (2001).
23. Tret'yakov E.V., et al. *Kvantovaya Elektron.*, **31**, 1095 (2001) [*Quantum Electron.*, **31**, 1095 (2001)].
24. Shuvalov V.V., et al. *Laser Phys.*, **12**, 627 (2002).